Boundary layer transition detection on a rotor blade using rotating mirror thermography

James Heineck
Photographic Technologist
Experimental Aero-physics Branch (AOX)
NASA Ames Research Center

Erich Schülein
Aerospace Engineer
Institute of Aerodynamics and Flow Technology
DLR Göttingen, Germany

Markus Raffel
Aerospace Engineer
Institute of Aerodynamics and Flow Technology
DLR Göttingen, Germany

Abstract

Laminar-to-turbulent transition on a rotor blade in hover has been imaged using an area-scan infrared camera. A new method for tracking a blade using a rotating mirror was employed. The mirror axis of rotation roughly corresponded to the rotor axis of rotation and the mirror rotational frequency is 1/2 that of the rotor. This permitted the use of cameras whose integration time was too long to prevent image blur due to the motion of the blade. This article will show the use of this method for a rotor blade at different collective pitch angles.

Introduction

Boundary layer turbulence causes minute surface temperature fluctuations when the ambient air is of a different temperature than the surface. The use of infrared cameras is an established technique for detecting the onset of turbulence for both fixed-wing wind tunnel testing and flight testing. The technique was first used in the 1960s and 1970s, particularly for re-entry vehicles where high enthalpy flows provide enough signal for the relatively insensitive cameras of the time. (NASA 1972; Schultz and Jones 1973). With the improvement in sensitivity, IR thermography has been used extensively in convective heat transfer applications. (Astarita et al. 2000). However, recent investigations have also been focused towards aerodynamic applications. In-flight thermography has been used for boundary layer transition detection and characterization by Brandon, et.al., (1990), Van Dam et al (1998), Banks, et.al., 2000 and 2012. Transition detection for a rotating aerodynamic experiment was done by Mori, et. al, in 2007. Contemporary IR thermography has the advantage of high temperature resolution (~0.02 K), as compared to Temperature Sensitive Paint, which has a precision of ~0.1 K, (Tropea, et. al., 2007).

Transition detection by high-speed infra-red (HSIR) thermography is manifested by rendering the surface-temperature differences induced by the different heat flux levels in laminar and turbulent flows as a change in brightness in a greyscale image. This change can be from light to dark, where the wall temperature is higher than the ambient air, or dark to light with the opposite wall-

Presented at the Fifth Decennial AHS Aeromechanics Specialists' Conference, San Francisco, CA, January 22-24, 2014.

to-air temperature difference. The first challenge in the low-speed flows, such as in these experiments, is the very small difference of these temperatures at adiabatic (equilibrium) wall conditions. For example, at 18 Hz rotation and *the* ambient temperature 298.0 K, the maximum wall temperature difference expected on the blade tip is only 0.066 K ($T_{ad,lam,R}$ = 299.406 K, $T_{ad,turb,R}$ = 299.472 K, $T_{0,R}$ = 299.65 K, M_R = 0.17). Limited heat capacity of the model material as well as the lateral heat conduction along the test surfaces further reduce the observed temperature differences on model surfaces in real tests.

The transition detection by IR thermography is best applied when either the model wall can be conditioned or the ambient air can be conditioned. The first technique, applied to helicopter blade flows by Richter & Schülein (2013), works only when the facility can rapidly change conditions to create a temperature difference between the wall and ambient air. This experiment heated the blades by spinning fast enough to heat the blades with flow-induced friction, then dropped the rotation speed for the measurements The thermal image makes clear transition detection possible only when the temperature differential is maintained. This experiment had only a short time for detection as the model and ambient temperature came to equilibrium. Similarly, in-flight experiments can control the aircraft temperature by either a high-altitude “cold-soaking” or a low altitude “heat-soaking” prior to the flight at experimental conditions.

In wind tunnels where the temperature is controlled by air exchangers or radiators, the ambient air temperature can be quickly changed relative to model temperature. But, like the case of the helicopter experiment above, the temperature differential decreases rapidly as the tunnel and model equilibrate

The second technique, used in the present work, heats the model with a radiative source, which in this case is a tungsten-filament spotlight. The image-subtraction method is employed, where images are made both with and without external surface heating. The laminar and turbulent regions on the model surfaces are revealed by subtracting the "cold" from "warm" thermal images. This method allows for long-duration experiments by establishing two sustained thermal states, a warm and a cold. As a result, the collection of large image databases for image averaging, subtraction and statistical analysis can be performed.

Experiments

Experiments were performed in a helicopter hover test facility. The chord and span of the four rotor blades were 54 mm and 510 mm respectively. The blades were untwisted, modified NACA0015 airfoils with blunt trailing edge and a square tip. The blades rotated at an angular velocity of 113.1 *rad/s* (18 rev/s) leading to a tip Mach number M = 0.17 and a Reynolds number at the tip Re = 2.4 x 10^5.

A mirror rotating at half the speed of the rotor was used to track the blade during recording, which had the effect of de-rotating the blade on the image sensor and allowed sharp imaging of the

whole blade. The image position was kept constant by a phase locked recording obtained by a stepper motor mirror drive (400 steps/rev) that was controlled by an optical encoder on the rotor axis (200 increments/rev). Different imaging configurations can be used in order to avoid motion blur (see Raffel and Heineck 2013). The recordings described hereafter were obtained where the axis of rotation of the mirror coincided with the axis of rotation of the rotor (Figure 1). The IR camera was installed upstream of the rotor model in order to detect the blades surface temperature on its suction side.

The measurements were made with the IRCAM Equus 327k L MCT (Mercury-Cadmium-Telluride) camera, which has a spectral range of 8.0-9.4 µm The focal plane array detector with 640×512 pixels and a pixel pitch of 24 µm. The shortest practical integration time was 5 µs and the highest full-resolution frame rate was 106 Hz. The integration time of the camera was set to 0.1 milliseconds during the experiments, which corresponds to ~6 mm of tip movement. A 50 mm, f/2 lens, which is "telephoto" for this sensor size, had a working distance which placed the camera and mirror far enough from the rotor disk to mitigate the camera's wake contaminating the inflow. A single row of self-adhesive trip dots, with 1.0 mm diameter and 0.145 mm thickness, were attached near the blade's leading edges. This was done to force transition so that the flow feature could be shown in the thermal image.

A 2.0 kW halogen spotlight was used as an external heating source. The intensity of external heating, or, more precisely, the radiative heat flux absorbed at the model surface, was high enough to achieve detectable temperature differences on the surface of the blades. Aerodynamic heating also occurs differentially along the span of the blade during rotation. This is an unwanted artifact that is eliminated with the subtraction technique.

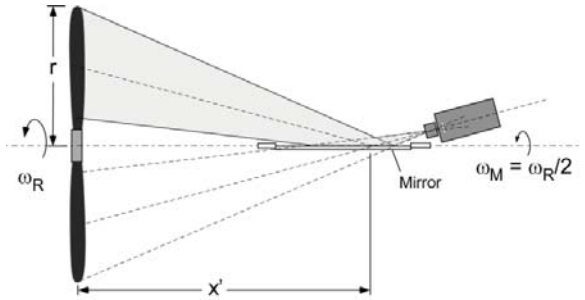

Fig. 1 Diagram of the mirror tracking method

PIV measurements

The acceleration of the air by the rotor disc causes downwash, which reduces the aerodynamic angle of attack of the rotor blade from the geometric angle of attack. In addition to the IR measurements, single-camera PIV recordings have been used in order to compute the effective angle of attack for each geometric angle of attack at 70% relative radial position. Additionally, this served to validate that the flow was attached for all test conditions. A schematic of the measurement region and measurement technique is shown in Figure 2.

Figure 3 depicts the measured velocity field in the laboratory frame of reference at r/R=0.70 for the geometric angles of attack, $\alpha = 7°$ ($\alpha_{eff} = 1.4°$), $\alpha = 10.5°$ ($\alpha_{eff} = 3.9°$) and $\alpha = 14°$ ($\alpha_{eff} = 5.7°$). The contours represent the

magnitude of the velocity field. Effects of flow separation have not been detected.

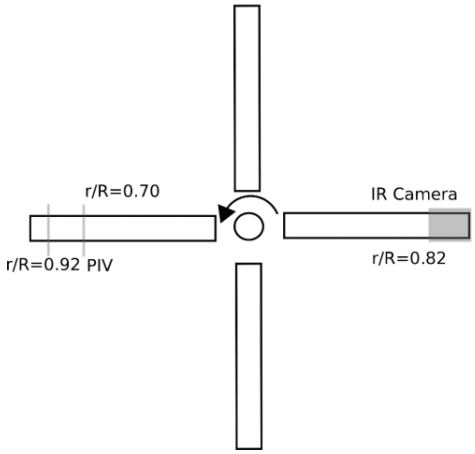

Fig. 2 Schematic representation of the location of thermography and PIV measurements. Blades are rotating in the counter clockwise direction

The effective angle of attack was determined by extracting the mean downwash velocities local to the leading edge of the blade. Figure 4 shows the geometric relationship between the downwash stream angle and the apparent blade angle-of-attack. The angle calculated from inverse tangent of the vertical and horizontal components of induced flow velocity. This value is subtracted from the pre-blade set angle-of-attack.

Results

Figure 5 are the image products that resulted from subtracting the "cold" image from the "hot" image of the suction side of a rotor blade at three different pitch angles. It can be seen that the image is sharp over the complete blade. A laminar region in the front of the blade (leading edge of the blade on the

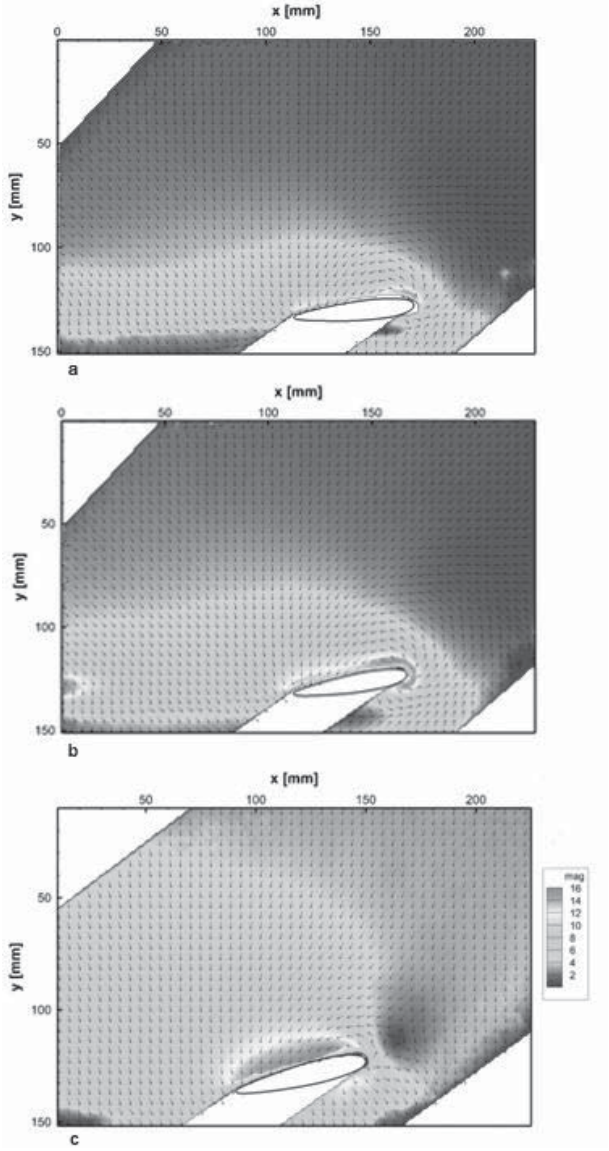

Fig. 3 Measured velocity field in the laboratory frame of reference at r/R=0.70 for various angles of attack: (Contours represent the magnitude of the velocity field.
(a): $\alpha = 7°$ ($\alpha_{eff} = 1.4°$), (b):$\alpha = 10.5°$ ($\alpha_{eff} = 3.9°$) and (c):$\alpha = 14°$ ($\alpha_{eff} = 5.7°$).

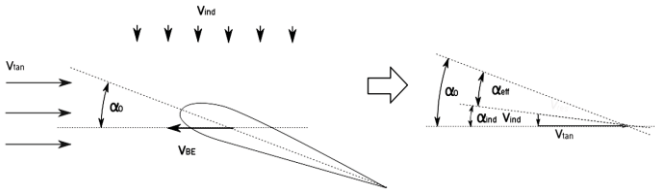

Fig. 4. Diagram of method for determining effective angle-of-attack.

left) can be identified by the higher image intensities. The transition line is located further upstream at higher pitch angles and closer to the tip (blade tip on the upper part). Darker regions downstream of the transition dots and downstream of the transition line indicate larger heat transfer (cooling, in this case) in the turbulent areas.

The intensity distributions were extracted at different radial positions and the transition onset and transition end were identified by an analysis of the intensity gradient in chord-wise direction. The transition positions extracted in this way agreed well with predictions from an Euler-boundary layer code called MSES, described by Drela (1990), with an envelope-e^N transition prediction and N = 5. Here the experimental "transition position" was taken to be half way between transition onset and transition end. The transition positions then agreed within x/c = 0.1 (see Fig.6).

Conclusion and outlook

The use of thermagraphy with a rotating mirror had been demonstrated as an effective method for detecting boundary layer transition. The results compared well to CFD results. Though this exeriment is a very early demostration of the technique it is anticipated it will scale to larger rotor experiments. A new mirror apparatus is being built with a servomotor and a 16-inch (406 mm) x 6-inch (150 mm) mirror. This dimension should accommodate larger rotor blades and longer working distances. Additionally, a software utility for test installation planning using this technique is being developed.

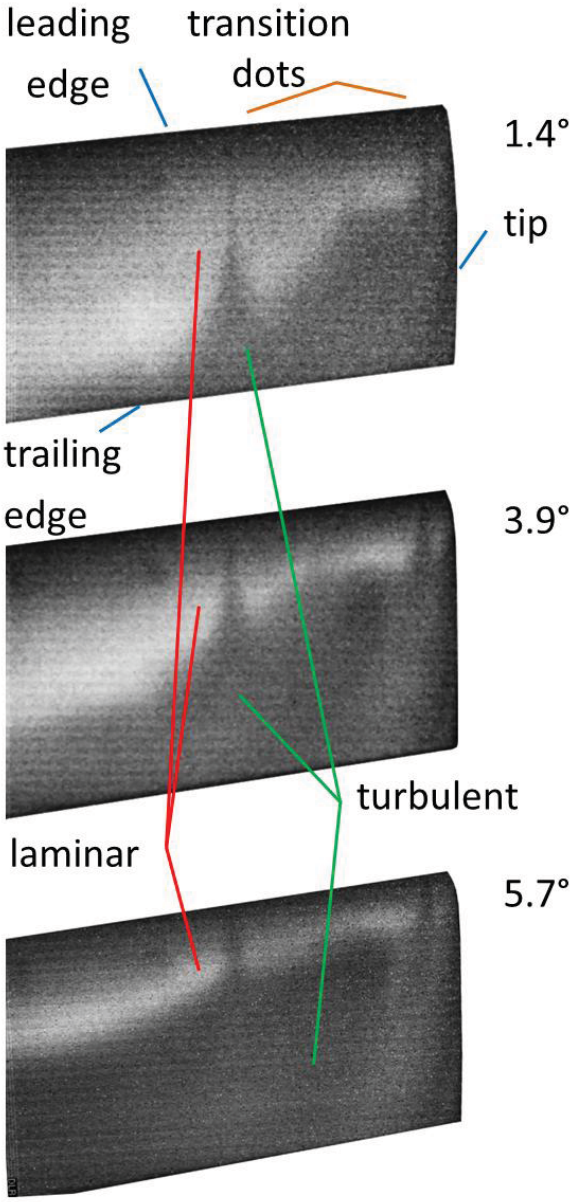

Fig. 5 Thermal images of blade at 1080 rpm. Collective pitches are (from top to bottom) $\alpha_{eff} = 1.4°$ deg, $\alpha_{eff} = 3.9°$, and $\alpha_{eff} = 5.7°$.

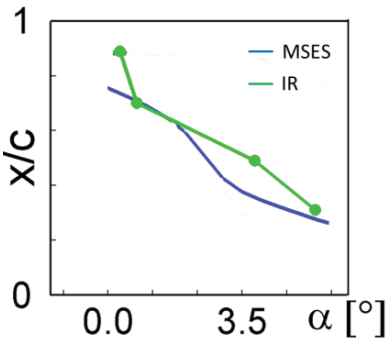

Fig. 6 Comparison of IR transition data with MSES

Acknowledgements

The help of our colleagues Anthony Gardner, Sathesh Mariappan, Waldemar Lang, Markus Krebs, Ed Schairer and Laura Kushner was greatly appreciated. This work was supported by the NASA Fundamental Aeronautics Program under the Aerosciences Project.

References

Hall, R.M., Obara, C.J., Carraway, D.L., Johnson, C.B., Wright, R.E., Jr., Covell, P.F., and Azzazy, M., "Comparisons of boundary-layer transition measurement techniques at supersonic Mach numbers," *AIAA Journal,* Vol. 29, No. 6, June 1991, pp. 865-879.

Brandon, J.M., Manuel, G.S., Wright, R.E., and Holmes, B.J., "In-flight flow visualization using infrared imaging," *Journal of Aircraft*, Vol. 27, July 1990, pp. 612-618.

Van Dam, C. P., Shiu, H. J. and Banks, D. W. "Remote in-flight boundary layer transition visualization using infrared thermography." 8th International Symposium on Flow Visualization, Sorrento, Italy, Sept. 1998.

D. W. Banks, C. P. van Dam, H. J. Shiu, and G. M. Miller, "Visualization of In-Flight Flow Phenomena Using Infrared Thermography", 9th International Symposium on Flow Visualization, Edinburgh, UK, Sept. 2000.

Astarita, T., Cardone, G., Carlomagno, G. M., and Meola, C.. "A survey on infrared thermography for convective heat transfer measurements." Optics & Laser Technology, Vol. 32, 2000, pp. 593-610,

Drela, M.. "Newton solution of coupled viscous/inviscid multielement airfoil flows", AIAA Paper 90-1470. AIAA, Fluid Dynamics, Plasma Dynamics and Lasers Conference. Seattle, WA., June,1990

NASA. 1972. "Space shuttle aerothermodynamics technology conference, Vol II: Heating." NASA-TM-X-2507.

Mori, M, Novac L., and Sekavčnik M., "Measurements on rotating blades using IR thermography." In Experimental Thermal and Fluid Science, Volume 32 (2), 2007, pp. 387–396.

Raffel, M., and Heineck, J. T. 2013. "Mirror based image de-rotation for aerodynamic rotor measurements," AIAA Journal in press.

Schultz, D.L, Jones, T.V. 1973. "Heat transfer measurements in short-duration hypersonic facilities," AGARDograph 165, AGARD.

Tropea, C., Yarin, A. L., and Foss, J. F. *Temperature, Concentration and Heat Flux,* Springer Handbook of Experimental Fluid Mechanics, New York: Springer, 2007.